BAREKENG: Journal of Mathematics and Its Applications
December 2026 Volume 20 Issue 4 Page 3405-3424
P-ISSN: 1978-7227 E-ISSN: 2615-3017
https://doi.org/10.30598/barekengvol20iss4pp3405-3424

HEAT AND MASS TRANSFER ANALYSIS ON MHD GO-AG-CUO-AL2O3/EG NANOFLUID FLOW PAST SHRINKING SHEET

Nooraini Zainuddin [1], Nur Syahirah Wahid [2], Iskandar Waini [3], Nor Ain Azeany Mohd Nasir [4*], Norihan Md Arifin [5], Norli Abdullah [6]

[1]Department of Applied Science, Faculty of Science, Management and Computing, Universiti Teknologi PETRONAS Seri Iskandar, Perak, 32610, Malaysia

[2,5]Department of Mathematics and Statistics, Faculty of Science, Universiti Putra Malaysia
[2]Institute of Nanoscience and Nanotechnology, Universiti Putra Malaysia
[4,5]Institute for Mathematical Research, Universiti Putra Malaysia
UPM Serdang, Selangor, 43400, Malaysia

[3]Fakulti Teknologi dan Kejuruteraan Industri dan Pembuatan, Universiti Teknikal Malaysia Melaka Hang Tuah Jaya, Durian Tunggal, Melaka, 76100, Malaysia

[4]Department of Mathematics, Centre for Defence Foundation Studies, Universiti Pertahanan Nasional Malaysia
[6]Department of Chemistry and Biology, Centre for Defence Foundation Studies,
Universiti Pertahanan Nasional Malaysia
Kem Sungai Besi, Kuala Lumpur, 57000, Malaysia

*Corresponding author's e-mail: * **norainazeany@upnm.edu.my***

Article Info

Article History:
Received: 27th October 2025
Revised: 03rd May 2026
Accepted: 07th June 2026
***Available online:** 24th August 2026*

Keywords:
Joule heating;
MHD;
Powell-Eyring model;
Stagnation point;
Tetra hybrid nanofluid;

ABSTRACT

This study discovers the mass and heat transfer characteristics of a magnetohydrodynamic GO-Ag-CuO-Al_2O_3/EG nanofluid streaming past a shrinking sheet under the force of various physical effects. The Powell-Eyring fluid model is engaged to account for the effect of a magnetic field, a stagnation point, viscous dissipation, radiation, Joule heating, and suction. Through similarity transformations, the governing partial differential equations are reduced to a system of ordinary differential equations, which are then resolved numerically using the bvp4c solver in MATLAB. The results affirmed that raising the heat transfer complements the thermal boundary layer, whereas reductions in the skin friction coefficient contribute to a reduction in drag force. Moreover, the velocity profile rises because of the shrinking effect, while the temperature profile decreases. The enhanced thermal conductivity provided by the quaternary nanoparticle suspension (GO-Ag-CuO-Al_2O_3) suggests that this fluid can maintain lower surface temperatures under high-heat flux conditions compared to mono or hybrid nanofluids. Consequently, these characteristics are particularly advantageous for electronic device cooling and heat exchangers in renewable energy systems where rapid heat dissipation is critical. Furthermore, the observed reduction in drag force under the influence of the magnetic field provides a theoretical basis for optimizing energy efficiency in magnetohydrodynamic pumps and metallurgical processing. These findings offer specific design parameters for boosting thermal management in industrial applications involving tetra-hybrid nanofluids.

How to cite this article:

N. Zainuddin, N. S. Wahid, I. Waini, N. A. A. M. Nasir, N. M. Arifin and N. Abdullah., "HEAT AND MASS TRANSFER ANALYSIS ON MHD GO-AG-CUO-AL2O3/EG NANOFLUID FLOW PAST SHRINKING SHEET", *BAREKENG: J. Math. & App.*, vol. 20, no. 4, pp. 3405-3424, Dec, 2026.

Journal homepage: *https://ojs3.unpatti.ac.id/index.php/barekeng/*
Journal e-mail: *barekeng.math@yahoo.com; barekeng.journal@mail.unpatti.ac.id*

Research Article · Open Access

1. INTRODUCTION

The rapid evolution of thermal systems across numerous industrial sectors has heightened the demand for advanced heat transfer fluids with superior thermal conductivity. In recent years, tetra-hybrid nanofluids, composed of four distinct nanoparticles suspended in a base fluid, have attracted significant interest due to their exceptional thermal, electrical, and chemical properties. The study by Mahariq et al. [1] found that tetra-hybrid nanofluids exhibit superior heat transfer performance compared to conventional single-component nanofluids. While the heat transfer rate of the tetra-hybrid nanofluid exhibited a 1.36% improvement compared to a conventional nanofluid, highlighting the superior thermal efficacy of Titanium dioxide (TiO_2), Copper (Cu), silver (Ag) and gold (Au) as tetra-hybrid nanofluids, particularly under radiative conditions, is reported by Zainab et al. [2]. Moreover, research in Fe_3O_4-Cu-TiO_2-$CoFe_2O_4$/sodium alginate has been carried out by Okash et al. [3], who demonstrated that an upsurge of the Stefan blowing parameter surpasses in enhancements within the mass and heat transfer rates as well as in velocity profile, while simultaneously causing reductions in both concentration and temperature profiles, indicating the significant influence of surface mass flux on transport characteristics. The findings of Rafique et al. [4] indicate a dual behaviour of the velocity profile, influenced by shrinking/stretching curvature, whereas the temperature increases consistently across both regimes. Meanwhile, an increment of 0.1 in the magnetic parameter results in a notable 1.4% improvement in the heat transfer ratio and a 17.3% growth within the skin friction coefficient, using TiO_2, silicon dioxide (SiO_2), Cu and alumina (Al_2O_3) as the tetra hybrid nanofluid is conveyed by Khashi'ie et al. [5]. Despite all the reports mentioned, one such combination, involving graphene oxide (GO), Ag, copper oxide (CuO), and Al_2O_3 in ethylene glycol (EG) as the base fluid, has shown great potential for energy systems, electronic cooling, and biomedical devices. GO bargains elevated surface area and extraordinary thermal conductivity, making it an effective agent in tetra-hybrid formulations. Nevertheless, while studies have reported improved heat transfer performance with tetra-hybrid nanofluids such as those by Arsad et al.[6], Abbas et al. [7] and Galal et al. [8], the literature on GO as a tetra-hybrid nanofluid remains sparse, particularly in the context of boundary layer flows. The combination of GO, Ag, CuO, and Al_2O_3 in ethylene glycol is selected to exploit the complementary thermal and stability characteristics of each component. GO delivers an extraordinary surface area and moderate thermal conductivity with outstanding dispersion stability. Ag offers exceptional thermal and electrical conductivity, improving heat transfer via electron transport. CuO offers reasonable conductivity and a high specific heat for energy storage, while Al_2O_3 enhances suspension stability and oxidation resistance. The synergy between carbon-based, metallic, and ceramic nanoparticles maximises both conductive and convective heat transfer performance, particularly under magnetohydrodynamic and non-Newtonian flow conditions.

In many engineering applications, fluids exhibit non-Newtonian behaviour due to the complex nature of materials such as polymers, slurries, and biological fluids. The Cross non-Newtonian fluid model is adopted by Sajid et al. [9] in their exploration of tetra-hybrid bio-nanofluid flow through a stenosed artery, incorporating convective heat transfer. Further investigation of other non-Newtonian fluids using the Xue model has been conducted by Sajid et al. [10]. The Xue model is also used by Abbas et al. [11] to investigate the flow and heat transfer of the Ellis tetra hybrid nanofluid. Meanwhile, the Phan-Thien-Tanner model is utilised by Paul and Das [12] to analyse the behaviour of non-Newtonian fluid (blood). There are several models for the investigation of non-Newtonian fluids that have been shown in the literature, such as the Yamada-Ota model by Das et al. [13], the tangent hyperbolic model by Amudhini and De [14], and the Jeffry model by Fatima et al. [15] However, none of them uses the Powell-Eyring model. The Powell–Eyring model, which stems from kinetic theory, is widely recognised for its ability to capture both shear-thinning and Newtonian characteristics under limiting conditions, without singularities at zero shear rates. This model has been successfully applied to simulate non-Newtonian flows in polymer processing, lubrication systems, and extrusion. Nevertheless, the interaction of Powell–Eyring fluids with tetra-hybrid nanoparticles remains unexplored.

Furthermore, the use of a magnetic field, commonly referred to as magnetohydrodynamics (MHD), introduces an additional mechanism for controlling the flow of conducting fluids. In the presence of a magnetic field, the flow behaviour is influenced by Lorentz forces, which can either suppress or enhance fluid motion, depending on the configuration. MHD flows of nanofluids have found diverse applications in metallurgy for controlling molten metal solidification, in nuclear reactor cooling for enhancing heat removal under magnetic fields, in electromagnetic casting processes, in MHD pumps for biomedical and microfluidic systems, and in advanced cooling technologies for high-power electronic and aerospace components, where precise thermal control is essential. The velocity profiles of both hybrid and tetra-hybrid nanofluids are observed by Khan et al. [16] to exhibit a decreasing trend with an upsurge in the magnetic field strength. The temperature profile of the tetra-hybrid nanofluid is enhanced by a magnetic field, as reported by Elboughdiri et al. [17]. A report by Majeed et al. [18] also agreed with the findings of Khan et al. [16] and Elboughdiri et al. [17]. This phenomenon is explained by Majeed et al. [18], who state that when a transverse magnetic field is applied, it generates a repulsive force that slackens the fluid motion and enhances the thermal profile. Other researchers have also reported significant findings on the application of a magnetic field to a tetra-hybrid nanofluid, including Gomathi and Poulomi [19], Yuan et al. [20] and Kumar et al. [21], to name a few. Basha et al. [22] investigated various fin placements in a hybrid nanofluid MHD flow and found that higher Rayleigh and Hartmann numbers, with 5% hybrid nanofluid, reduce heat transfer by 110%. The inclined MHD, together with nanoparticle concentration and heat source/sink, has a major influence on heat transfer, as suggested by Thirumalaisamy and Reddy [23]. The combination of MHD and a nanoparticle concentration of about 5% can increase the heat transfer ratio, as reported by Thirumalaisamy et al. [24]. Previously, a ternary hybrid nanofluid based on kerosene and the effect of MHD was reported to have increased the heat transfer rate by almost 38%, as reported by Kim et al. [25].

Joule heating, which appears because of the conversion of electrical energy into thermal energy in conductive fluids, further complicates the energy equation in MHD flows. In high-temperature systems or in the presence of electrical current, this phenomenon cannot be neglected. The inclusion of joule heating in nanofluid models has proven critical for improving simulation accuracy in microelectronic cooling, MHD pumps, and electroconductive fluid applications. Research on angioplasty is conducted by Paul et al. [26] involving a balloon catheter and nanoparticles in arteries under the influence of Joule heating with a tetra hybrid nanofluid, revealing that an increase in the catheter's height enhances blood velocity in the central annular region. In contrast, a dense interfacial nanolayer leads to a reduction in both blood temperature and heat transfer. While temperature and velocity profiles are observed by Mumtaz et al. [27] being dominated by the specific type of nanofluid employed, highlighting the critical role of nanofluids in the presence of a magnetic field and heat source/sink for optimising both heating and cooling applications. A growth in the Eckert number (Ec) is noted by Swami et al. [28] surpassing in an upsurge within the temperature profile, attributed to intensified viscous dissipation that generates additional thermal energy within the fluid. In contrast, a decline in the temperature profile with the rise of both the Prandtl number and the intensity of the heat source is detected by Lakshmi and Murty [29]. However, several studies have accounted for joule heating in nanofluids, for example, in a ternary hybrid nanofluid by Wang et al.[30], Tanveer et al. [31], and Iqbal et al. [32], while hybrid nanofluid by Safa et al. [33], its impact in the context of tetra-hybrid nanofluids with non-Newtonian behavior has not yet been systematically addressed. However, the synergistic impact of quaternary nanoparticle interactions within a non-Newtonian (Powell-Eyring) framework under the simultaneous influence of Joule heating and thermal radiation remains unexplored. This study fills this critical gap by providing a more sophisticated mathematical model that accounts for the combined shear-thinning/thickening characteristics and the enhanced electrical conductivity of the GO-Ag-CuO-Al_2O_3 suspension, which are essential for predicting precise thermal behaviors in high-energy MHD systems.

The findings of this study offer a direct contribution to the design of next-generation thermal management systems. For instance, integrating Joule heating and tetra-hybrid conductivity enables more accurate efficiency predictions for power conversion systems using conductive fluids in MHD power generators. While for advanced microelectronics, the Powell-Eyring parameters and nanoparticle concentration influence on cooling rates are identified, the work provides a roadmap for preventing thermal runaway in high-density processors. Moreover, in precision metallurgy, the ability to control the velocity profile through magnetic field modulation in a tetra-hybrid medium facilitates more uniform cooling in metal extrusion and polymer coating processes, directly improving product structural integrity.

Based on the preceding literature, it is evident that the synergistic role of carbon-based (GO), metallic (Ag), and ceramic (CuO, Al_2O_3) nanoparticles in a quaternary suspension remains under-researched. The primary novelty of this work lies in the integration of the Powell–Eyring non-Newtonian framework with a GO–Ag–CuO–Al_2O_3/EG tetra-hybrid nanofluid under the simultaneous influence of MHD, Joule heating, and thermal radiation. While separate components of these phenomena have been studied, their combined impact over a shrinking surface—particularly regarding the conversion of electrical energy into thermal energy—has not yet been addressed. This research aims to fill this gap by developing a robust mathematical model solved via the MATLAB [34] bvp4c solver. The resulting insights into velocity, temperature, and transport coefficients provide critical design parameters for high-performance thermal management in electronics, advanced energy systems, and industrial cooling processes.

2. RESEARCH METHODS

2.1 Mathematical Modelling

Assume that a tetra hybrid nanofluid consisting of graphene oxide (GO), silver (Ag), copper oxide (CuO) and alumina (Al_2O_3) are uniformly dispersed and diluted with ethyl glycol (EG) is incompressible and steady (laminar) flowing over a horizontal shrinking sheet as shown in Fig. 1. x represents the horizontal Cartesian coordinate measured along the surface of the shrinking sheet, starting from the stagnation point and y represents the vertical Cartesian coordinate measured the normal (perpendicular) to the surface. Referring to Waini et al.[36], the surface velocity is known as $u_w = \alpha x^{1/3}$ where α is a positive constant, and the mass velocity is denoted as v_w, while the far-field velocity is known as $u_e = \varepsilon x^{1/3}$. It is also presumed that the surface temperature noted as $T_w = T_0 x^{2/3} + T_\infty$ as T_∞ and T_0 are the far-field and reference temperature, respectively. The effects of the magnetic field given as $B_x = B_0 x^{-1/3}$ is non-uniform and depends on the axial position to ensure the existence of a similarity solution, and radiative heat flux follows the Rosseland approximation, $q_r = -\left(\frac{4\sigma *}{3k *}\right)\frac{\partial T^4}{\partial y}$, where the temperature difference within the flow is assumed to be sufficiently small such that $T^4 \cong 4T_\infty^3 T - 3T_\infty^4$ with B_o is a magnetic strength constant, $\sigma *$ denoted as Stefan-Boltzmann and $k *$ known as Rosseland mean absorption are considered in the system.

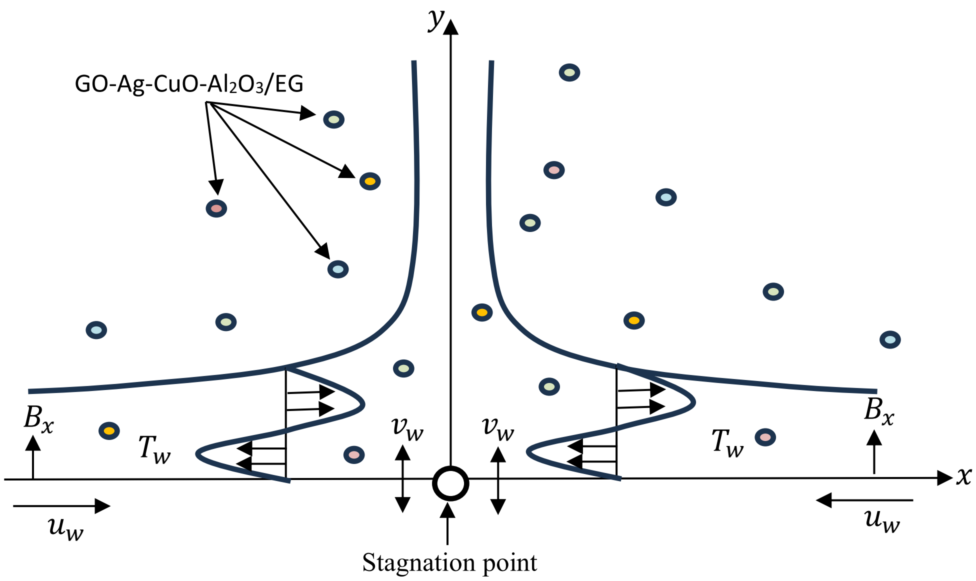

Figure 1. Illustration of The Flow Model

Based on the assumption above, the governing equations in [35] with the appropriate boundary conditions (BC) [36] involved in the system are given by

$$\frac{\partial u}{\partial x} + \frac{\partial v}{\partial y} = 0, \tag{1}$$

$$\frac{u\partial u}{\partial x} + \frac{v\partial u}{\partial y} = u_e \frac{du_e}{dx} + v_{Tehnf}\frac{\partial^2 u}{\partial y^2} + \frac{1}{\rho_{Tehnf}\beta\epsilon}\frac{\partial^2 u}{\partial y^2} - \frac{1}{2\rho_{Tehnf}\beta\epsilon^3}\left(\frac{\partial u}{\partial y}\right)^2 \frac{\partial^2 u}{\partial y^2} - \frac{\sigma_{Tehnf}B_x^2}{\rho_{Tehnf}} u, \tag{2}$$

$$\text{BC: } u = \lambda u_w \ , \quad v = v_w \ , \quad at \quad y = 0, \ u \to u_e \ , \ as \quad y \to \infty,$$

$$\frac{u\partial T}{\partial x} + \frac{v\partial T}{\partial y} = \frac{k_{Tehnf}}{(\rho c_p)_{Tehnf}}\frac{\partial^2 T}{\partial y^2} + \frac{\mu_{Tehnf}}{(\rho c_p)_{Tehnf}}\left(\frac{\partial u}{\partial y}\right)^2 - \frac{1}{(\rho c_p)_{Tehnf}}\frac{\partial q_r}{\partial y} + \frac{\sigma_{Tehnf}B_x^2}{(\rho c_p)_{Tehnf}} u^2 \ , \tag{3}$$

$$\text{BC: } \ T = T_w, \ at \quad y = 0, \quad T \to T_\infty \quad as \quad y \to \infty.$$

The parameters associated with Eqs. (1)-(3) are u and v will known as velocity components in x and y axes, and the remaining parameters are listed in Table 1.

Table 1. Parameters Associated with Eqs. (1)-(3)

Symbol	Parameter	Unit (SI)
ν_{Tehnf}	Kinematic viscosity	$\frac{m^2}{s}$
ρ_{Tehnf}	Density	$\frac{kg}{m^3}$
β	Powell-Eyring fluid parameter (dimensionless)	-
ϵ	Powell-Eyring fluid parameter (Material constant)	s^{-1}
σ_{Tehnf}	Electrical conductivity	$\frac{S}{m}$
k_{Tehnf}	Thermal conductivity	$\frac{W}{m\cdot K}$
$(\rho c_p)_{Tehnf}$	Heat capacity (volumetric)	$\frac{J}{m^3\cdot K}$
μ_{Tehnf}	Dynamic viscosity	$\frac{kg}{m\cdot s}$
λ	Stretching ($\lambda > 0$) / Shrinking ($\lambda < 0$)	-

The subscript $Tehnf$ stands for tetra-hybrid nanofluid which is representing the composite properties of the Ag (ϕ_1), Al_2O_3 (ϕ_2), CuO (ϕ_3), and GO (ϕ_4) as well as the total concentration ratio for tetra-hybrid nanofluid is given as $\varphi_{Tehnf} = \phi_1 + \phi_2 + \phi_3 + \phi_4$.

2.2 Tetra Hybrid Nanofluid

The mathematical framework of this study is built upon several physical assumptions. A primary limitation is the neglect of velocity and thermal slip between the nanoparticles and the base fluid, assuming a perfect continuum. Furthermore, the model assumes negligible inter-particle interactions and a homogeneous distribution of the quaternary phases (GO, Ag, CuO, and Al_2O_3). In practical applications, however, the varying surface charges and morphologies of these four distinct materials may lead to nanoparticle agglomeration or sedimentation over time. Despite these simplifications, the chosen combination offers unique synergistic benefits: GO provides ultrahigh thermal conductivity, Ag offers metal-level heat transfer enhancement, CuO serves as a stable conductor, and Al_2O_3 acts as a structural stabilizer to minimize sedimentation. These properties, quantified in Table 2, provide a high-performance theoretical baseline for tetra-hybrid nanofluid behavior.

Table 2. Related Formulas for Thermophysical Properties of Tetra Hybrid Nanofluid.

Thermophysical Properties	Tetra Hybrid Nanofluid [26]
μ	$\frac{\mu_{Tehnf}}{\mu_f} = \frac{1}{(1-\phi_1)^{2.5}(1-\phi_2)^{2.5}(1-\phi_3)^{2.5}(1-\phi_4)^{2.5}}$
ρ	$\frac{\rho_{Tehnf}}{\rho_f} = (1-\phi_4)\left((1-\phi_3)\left((1-\phi_2)\left((1-\phi_1)+\frac{\phi_1\rho_1}{\rho_f}\right)+\frac{\phi_2\rho_2}{\rho_f}\right)+\frac{\phi_3\rho_3}{\rho_f}\right)+\frac{\phi_4\rho_4}{\rho_f}$
σ	$\frac{\sigma_{Tehnf}}{\sigma_f} = \left(\frac{(1+2\phi_4)\sigma_4+(1-2\phi_4)\sigma_{thnf}}{(1-\phi_4)\sigma_4+(1-\phi_4)\sigma_{thnf}}\right)\frac{\sigma_{thnf}}{\sigma_f}$, $\frac{\sigma_{thnf}}{\sigma_f} = \left(\frac{(1+2\phi_3)\sigma_3+(1-2\phi_3)\sigma_{hnf}}{(1-\phi_3)\sigma_3+(1-\phi_3)\sigma_{hnf}}\right)\frac{\sigma_{hnf}}{\sigma_f}$, $\frac{\sigma_{hnf}}{\sigma_f} = \left(\frac{(1+2\phi_2)\sigma_2+(1-2\phi_2)\sigma_{nf}}{(1-\phi_2)\sigma_2+(1-\phi_2)\sigma_{nf}}\right)\frac{\sigma_{nf}}{\sigma_f}$, $\frac{\sigma_{nf}}{\sigma_f} = \left(\frac{(1+2\phi_1)\sigma_1+(1-2\phi_1)\sigma_f}{(1-\phi_1)\sigma_1+(1-\phi_1)\sigma_f}\right)$
k	$\frac{k_{Tehnf}}{k_f} = \left(\frac{k_4+2k_{thnf}-2\phi_4(k_{thnf}-k_4)}{k_4+2k_{thnf}+\phi_4(k_{thnf}-k_4)}\right)\frac{k_{thnf}}{k_f}$, $\frac{k_{thnf}}{k_f} = \left(\frac{k_3+2k_{hnf}-2\phi_3(k_{hnf}-k_3)}{k_3+2k_{hnf}+\phi_3(k_{hnf}-k_3)}\right)\frac{k_{hnf}}{k_f}$,

Thermophysical Properties	Tetra Hybrid Nanofluid [26]
	$\frac{k_{hnf}}{k_f}=\left(\frac{k_2+2k_{nf}-2\phi_2(k_{nf}-k_2)}{k_2+2k_{nf}+\phi_2(k_{nf}-k_2)}\right)\frac{k_{nf}}{k_f},\ \frac{k_{nf}}{k_f}=\left(\frac{k_1+2k_f-2\phi_1(k_f-k_1)}{k_1+2k_f+\phi_1(k_f-k_1)}\right)$
ρc_p	$\frac{(\rho c_p)_{Tehnf}}{(\rho c_p)_f}=(1-\phi_4)\left((1-\phi_3)\left((1-\phi_2)\left((1-\phi_1)+\frac{\phi_1(\rho c_p)_1}{(\rho c_p)_f}\right)+\frac{\phi_2(\rho c_p)_2}{(\rho c_p)_f}\right)+\frac{\phi_3(\rho c_p)_3}{(\rho c_p)_f}\right)+\frac{\phi_4(\rho c_p)_4}{(\rho c_p)_f}$

The values incorporated with the tetra nanoparticles thermophysical properties are given as Table 3. All the values tabulated are at temperature of 300K.

Table 3. The Values for Thermophysical Characteristics of GO, Ag, CuO, Al_2O_3 and EG at 300K ([35] - [40]).

Properties	GO	Ag	CuO	Al_2O_3	Ethylene Glycol
References	[35]	[38]	[40]	[37]	[35], [39]
Dynamic viscosity $(kgm^{-1}s^{-1})$	-	-	-	-	0.0159
Density (kgm^{-3})	1800	10490	6310	3880	1113
Electrical conductivity (Sm^{-1})	1.0×10^{-8}	6.30×10^{7}	1.5×10^{3}	1.0×10^{-12}	1.7×10^{-5}
Thermal conductivity $(Wm^{-1}K^{-1})$	72	429	33	36	0.256
Specific Heat capacity $(Jkg^{-1}K^{-1})$	531	235	532.7	773	2433

3. RESULTS AND DISCUSSION

The governing equation complexity is then scaled down using similarity variables to reduce the governing equations into third-order ordinary differential equations (ODEs). Then, the higher-order ODEs will be reduced into first-order ODEs to solve using the bvp4c solver in MATLAB. The solutions will be validated by comparing them with previously established results in the literature. The skin friction coefficient $Re_x^{1/2}C_f$, local Nusselt number $Re_x^{-1/2}Nu_x$, velocity $f'(\eta)$ and temperature $\theta(\eta)$ analysis will be carried out and discussed further.

3.1 Reduced Ordinary Differential Equations

The similarity variables given as Waini et al. [36]

$$\Psi=\sqrt{\alpha\nu_f}\,x^{\frac{2}{3}}f(\eta),\qquad \vartheta=\frac{T-T_\infty}{T_w-T_\infty},\quad \eta=\frac{y}{x^{\frac{1}{3}}}\sqrt{\frac{\alpha}{\nu_f}},\tag{4}$$

with ν_f is the kinematic viscosity of base fluid, η and ϑ are similarity variable (dimensionless) associated with stream function Ψ. Utilizing Eq. (4), the velocity components are then becoming

$$u=\frac{\partial\Psi}{\partial y}=\alpha\,x^{1/3}f'(\eta),\qquad v=-\frac{\partial\Psi}{\partial x}=-\sqrt{\alpha\nu_f}\,x^{-\frac{1}{3}}\left(\frac{2}{3}f(\eta)-\frac{1}{3}\eta f'(\eta)\right),\tag{5}$$

where the derivative for all parameters associated with Eqs. (1)-(3) are $\frac{\partial u}{\partial x}=\frac{1}{3}\alpha\,x^{-\frac{2}{3}}(f'-f''\eta)$, $\frac{\partial u}{\partial y}=\alpha\sqrt{\frac{\alpha}{\nu_f}}f''$, $\frac{\partial^2u}{\partial y^2}=\frac{\alpha^2}{\nu_f}x^{-1/3}f'''$, $\frac{\partial v}{\partial y}=-\frac{1}{3}\alpha\,x^{-\frac{2}{3}}(f'-\eta f'')$, $\frac{\partial T}{\partial x}=-\frac{1}{3}T_0\,y\,x^{-\frac{2}{3}}\sqrt{\frac{\alpha}{\nu_f}}\vartheta'+\frac{2}{3}T_0x^{-\frac{1}{3}}\vartheta$, $\frac{\partial T}{\partial y}=T_0\,x^{1/3}\sqrt{\frac{\alpha}{\nu_f}}\vartheta'$.

Based on Aminuddin et al. [35], the expression $f(\eta)-\frac{1}{2}\,\eta\, f'(\eta)$ can be simplified as S, when its positives known as suction while when its negatives known as injection. Hence, the mass velocity on the sheet represents as $v_w=-\frac{2}{3}\sqrt{\alpha v_f}\,x^{-\frac{1}{3}}S$. Substituting Eqs. (4) and (5) into the governing Eqs. (1)-(3), the resultant equations as follows,

$$\frac{1}{3}\Gamma^2+\frac{A_1}{A_2}f'''+\frac{\xi}{A_2}f'''-\frac{\xi\varpi}{A_2}f'''f''^2-\frac{A_3}{A_2}M\left(f'-\Gamma\right)+\frac{2}{3}ff''-\frac{1}{3}f'^2=0, \tag{6}$$

$$\text{BC: } f(0)=S,\quad f'(0)=\lambda \;\; as\,\eta=0,\; f'(\eta)\to\Gamma \;\; as\,\eta\to\infty,$$

$$\frac{A_4}{A_5}\frac{1}{Pr}\vartheta''+\frac{A_1}{A_5}Ec\,f''^2+\frac{4}{3}\frac{1}{A_5}\frac{R}{Pr}\vartheta''+\frac{A_3}{A_5}M\,Ec\,f'^2-2\frac{A_3}{A_5}M\,Ec\,\Gamma f'+\frac{A_3}{A_5}M\,Ec\,\Gamma^2 -\frac{2}{3}\vartheta f'+\frac{2}{3}\vartheta' f=0, \tag{7}$$

$$\text{BC: } \vartheta(0)=1 \;\; as\,\eta=0,\; \vartheta(\eta)\to 0 \;\; as\,\eta\to\infty.$$

The parameters associated with Eqs. (6)-(7) are:

$$\xi=\frac{1}{\rho_f\beta\epsilon v_f},\quad \varpi=\frac{\alpha^3}{2\,\epsilon^2 v_f},\quad \Pr=\frac{\mu_f c_{p_f}}{k_f},\quad A_1=\frac{\mu_{Tehnf}}{\mu_f},$$
$$A_2=\frac{\rho_{Tehnf}}{\rho_f},\quad A_3=\frac{\sigma_{Tehnf}}{\sigma_f},\quad A_4=\frac{k_{Tehnf}}{k_f},\quad A_5=\frac{(\rho c_p)_{Tehnf}}{(\rho c_p)_f}, \tag{8}$$
$$Ec=\frac{\alpha^2}{T_0 c_{p_f}},\quad R=\frac{4\sigma * T_\infty^3}{k * k_f},\; M=\frac{\sigma_f B_0^2}{\alpha\rho_f},\; \Gamma=\frac{\varepsilon}{\alpha}.$$

The values for tetra hybrid nanofluid parameters A_1, A_2, A_3, A_4, A_5 can be calculated using the formula given in Table 2 which are different from Takabi and Salehi [41].

The significant engineering quantities namely Nusselt number Nu_x and skin friction C_f are expressed as Waini et al. [36],

$$C_f=\frac{\tau_w}{\rho_{Tehnf}u_w^2}=\frac{\left[\left(\mu_{Tehnf}+\frac{1}{\beta\epsilon}\right)\frac{\partial u}{\partial y}-\frac{1}{6\beta\epsilon^3}\left(\frac{\partial u}{\partial y}\right)^3\right]_{y=0}}{\rho_{Tehnf}u_w^2},$$
$$Nu_x=\frac{x\,q_w}{k_{Tehnf}(T_w-T_\infty)}=\frac{x\left[-k_{Tehnf}\left(\frac{\partial T}{\partial y}\right)_{y=0}+(q_r)_{y=0}\right]}{k_{Tehnf}(T_w-T_\infty)}, \tag{9}$$

with wall shear stress is noted as τ_w and heat flux denote as q_w. Hence, after substituting Eqs. (4) and Eq. (5) into Eq. (9) will produce $Re_x^{1/2}C_f$ as well as $Re_x^{-1/2}Nu_x$ along with local Reynolds number $Re_x=\frac{x\,u_w}{v_f}$ as follows,

$$Re_x^{1/2}C_f=\left(\frac{A_1}{A_2}f''(0)+\frac{\xi}{A_2}f''(0)-\frac{1}{3}\frac{\xi\varpi}{A_2}f''^3(0)\right),\qquad Re_x^{-1/2}Nu_x=-\left[A_4+\frac{4}{3}R\right]\vartheta'(0). \tag{10}$$

3.2 Numerical Approach

As we can see from Eqs. (6)-(7), the transformed ODEs are nonlinear and coupled which it makes more complex to solve using analytical method. Hence, it is wise to use the numerical method in solving Eqs. (6)-(7). Therefore, in this research, Eqs. (6)-(7) are solved using MATLAB software due to the fact that this software is user-friendly and reliable. Eqs. (6)-(7) is constructed from implementing the similarity transformation process which producing a two-point boundary value problem. Since the problem is in two-point boundary value problem, bvp4c solver is more suitable in solving this problem. The bvp4c solver uses a 3-stage Lobatto formula (collocation method) with 4th order accuracy. The tolerance chosen to solve this problem is $RelTol = 10^{-10}$ to ensure the accuracy and convergence of the computed solutions. The domain for this problem is $\eta = 15$ to make sure in capturing the asymptotic behaviour of the computed solutions.

Eqs. (6)-(7) are then reduced into first order ODEs to comply with the nature of the bvp4c solver. The equations constructed as:

$$\begin{gathered} d_1 = f, \\ d_2 = f', \\ d_3 = f'', \\ \frac{1}{3}\Gamma^2 + \frac{A_1}{A_2} d_3' + \frac{\xi}{A_2} d_3' - \frac{\xi\varpi}{A_2} d_3' d_3^2 - \frac{A_3}{A_2} M\,(d_2 - \Gamma) + \frac{2}{3} d_1 d_3 - \frac{1}{3} {d_2}^2 = 0 \\ \text{BC.: } d_{1a} = S,\quad d_{2a} = \lambda, d_{2b} = \Gamma, \end{gathered} \tag{11}$$

$$\begin{gathered} d_4 = \vartheta, \\ d_5 = \vartheta', \\ \frac{A_4}{A_5}\frac{1}{Pr} d_5' + \frac{A_1}{A_5} Ec\, {d_3}^2 + \frac{4}{3}\frac{1}{A_5}\frac{R}{Pr} d_5' + \frac{A_3}{A_5} M\, Ec\, {d_2}^2 - 2\frac{A_3}{A_5} M\, Ec\, \Gamma d_2 + \frac{A_3}{A_5} M\, Ec\, \Gamma^2 \\ - \frac{2}{3} d_4 d_2 + \frac{2}{3} d_5 d_1 = 0, \\ \text{BC.: } d_{4a} = 1, d_{4b} \to 0\,. \end{gathered} \tag{12}$$

where S is suction/injection parameter, d_{1a} is $f(0)$, d_{2a} is $f'(0)$, d_{2b} noted as $f'(\eta)$, d_{4a} is $\vartheta\,(0)$ and d_{4b} is $\vartheta(\eta)$.

Eqs. (11)-(12) yield two possible sets of solutions. To determine which solution is physically meaningful, a stability analysis is essential. Stability analysis investigates the behavior of the system when slightly perturbed from the equilibrium state. To determine the physical reliability of the dual solutions, a stability analysis is performed by considering the unsteady form of the governing equations. Following the formulation by Waini et al. [36], we introduce a time-dependent dimensionless variable $\tau = \alpha x^{-2/3} t$ and the defined perturbed flow are $f(\eta,\tau) = f_0(\eta) + e^{-\gamma\tau} F(\eta,\tau)$ and $\theta(\eta,\tau) = \theta_0(\eta) + e^{-\gamma\tau} G(\eta,\tau)$ where γ is the unknown eigenvalue. The stability of the steady-state solution (f_0, θ_0) is determined by the smallest eigenvalue γ_1. A positive value ($\gamma_1 > 0$) indicates an initial decay of perturbations, signifying a stable flow, whereas a negative value ($\gamma_1 < 0$) indicates growth of disturbances, signifying an unstable flow. Given that the core similarity structure of the present shrinking sheet model aligns with the established framework in Waini et al. [36], the first solution is identified as stable, while the second is physically unrealizable.

The model from Eqs. (11)-(12) are considered radiation, suction and joule heating parameters. R governs heat transfer by thermal radiation, which can alter the temperature distribution in the boundary layer while M and Joule heating effect increase fluid temperature through Lorentz forces and Ohmic dissipation. Meanwhile, Ec viscous heating, while suction reduces boundary layer thickness and enhances heat and mass transfer rates. The solution obtained from Eqs. (11)-(12) are being compared to Waini et al. [36] and Cortell [42] for validation. Based on Table 4, the comparison shown our present solutions are similar to Waini et al. [36] and Cortell [42]. Hence, the solutions are reliable.

Table 4. Comparison of f'' (0) with [36] and [42] when $\lambda = 1, \Gamma = \xi = \varpi = M = 0$

S	[36]	[42]	**Present results**
-0.75	-	-0.453521	-0.453632072
-0.5	-0.518869	-0.518869	-0.518961864
0	-0.677648	-0.677647	-0.677695754
0.5	-0.873643	-0.873627	-0.873658093
0.75	-	-0.984417	-0.984446588

The value of Pr is calculated using following formula [43],

$$Pr = \frac{\mu_f c_{pf}}{k_f}. \tag{13}$$

To minimize the model's complexity Eqs. (6)-(7), several parameters are fixed to $\lambda = -1.8, \Gamma = 1, S = 2.0$. The concentration for tetra hybrid nanofluid are fixed to $\phi_1 = 0.01$ (Ag), $\phi_2 = 0.01$ (Al_2O_3), $\phi_3 = 0.01$ (CuO) and $\phi_4 = 0.003, 0.005, 0.006$ (GO). These values are chosen based on Ma et al. [44] reported that the low volume fraction less than 1% can avoid strong viscosity rise and agglomeration while enhancing thermal. GO effectively at low concentration because of large surface area without destabilizing the suspension is reported by Balaji et al. [45]. The parameters that will be varies are $M = 0.0, 0.5, 1.0, 1.5, Ec = 0.1, 0.2, 0.3, R = 0.0, 0.5, 1.0, 1.5$, $\xi = \varpi = 0.001, 0.01, 0.1$. M was varied from 0 to 1.5 to represent weak-to-moderate transverse magnetic fields typical in MHD cooling and metallurgical applications and to cover the range most commonly explored in numerical MHD nanofluid studies while Ec was kept small because the studied configuration (boundary-layer cooling with moderate velocities) corresponds to low-to-moderate viscous dissipation; such Ec ranges are widely used to study viscous-heating effects without driving the solution into unphysical high-temperature regimes. Furthermore, R was taken in the range 0 to 1.5 to represent environments from negligible to moderate radiative transfer (electronics cooling to higher radiative environments). Finally, ξ, ϖ were chosen within small-to-moderate values to capture realistic non-Newtonian shear-thinning behavior observed in polymeric and rheological fluids, while ensuring the model remains physically valid and the numerical solver remains stable. These ranges are consistent with prior numerical studies on Powell–Eyring nanofluid flows and allow direct comparison with literature results.

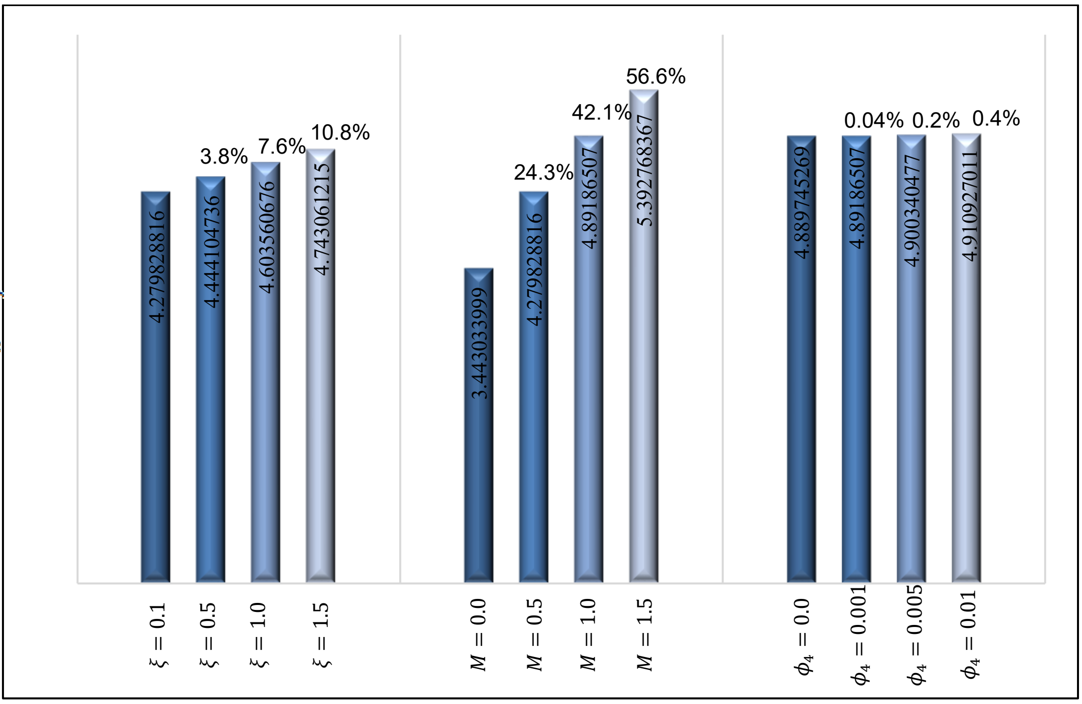

Figure 2. The Values of $Re_x^{1/2} C_f$ for Several Parameters

The Powell–Eyring fluid model accounts for non-Newtonian characteristics in a flow and governs the degree of the non-linearity. As shown in Fig. 2, a growth in the Powell–Eyring parameter (ξ) from 0.1 to 1.5 results in a remarkable increase about 10% in $Re_x^{1/2} C_f$ at the surface. Physically, a higher ξ implies that the fluid behaves less viscously near the wall, which enhances the fluid's resistance to motion. The presence of the Powell–Eyring nonlinearity reinforces this resistance by making the velocity gradient steeper near the wall. The increased $Re_x^{1/2} C_f$ denoted a closer and dense boundary layer, exclusively when combined with suction and magnetic effects.

A rise in magnetic parameter (M) from 0.0 to 1.5 manages to a major growth about 56% in the $Re_x^{1/2} C_f$, as reflected in Fig. 2. This behavior can be physically attributed to the Lorentz force, which is created when an electrically conducting fluid flows through a magnetic field. This force turns a contrary to the direction of fluid motion, thereby increasing the resistance to flow. As a result, an extreme velocity gradient develops near the wall, which increases the shear stress, and consequently, the skin friction. The presence of M amplifies shear near the wall by intensifying the non-linear velocity gradient. This leads to a combined effect that enhances wall shear stress and $Re_x^{1/2} C_f$ even further.

From Fig. 2, the current analysis of MHD GO–Ag–CuO–Al_2O_3/EG hybrid nanofluid flow past a shrinking sheet, a slight increase about 0.4% in the $Re_x^{1/2} C_f$ is observed as the GO concentration parameter (ϕ_4) improves from 0.001 to 0.01 compared to Ag–CuO–Al_2O_3/EG hybrid nanofluid (when $\phi_4 = 0.0$). GO is known for its exceptionally high thermal conductivity and large surface area. When added into the base nanofluid consisting of Ag, CuO, and Al_2O_3 nanoparticles suspended in ethylene glycol, GO contributes to the enhancement of the effective viscosity and momentum diffusivity of the fluid. This increase in viscosity leads to greater resistance near the wall, causing a modest rise in shear stress, hence the slight increase in $Re_x^{1/2}C_f$. It is widely known that Ag exhibit extremely high thermal and electrical conductivity which can promote rapid heat dispersion with less impact towards viscosity rather than GO. While CuO can contribute to thermal energy storage due to its higher specific heat and Al2O3 will enhance the suspension stability of the mixture due to its stability and low cost. The Powell–Eyring fluid non-Newtonian temperament captures shear-thinning behavior, which is sensitive to changes in nanoparticle concentration. As ϕ_4 rises, the shear-thinning nature becomes more pronounced due to microstructural interactions among nanoparticles, marginally increasing near-wall resistance. With significant viscous dissipation, internal energy increases, will leading to higher temperatures. However, the role of GO in improving heat conduction indirectly stiffens the velocity gradient near the wall, thus contributing slightly to increased $Re_x^{1/2}C_f$. Though the influence is minor, it emphasizes the significance of optimizing ϕ_4 to balance the enhancement of thermal performance with adequate flow resistance in practical applications such as polymer processing, thermal coatings, and MHD cooling systems.

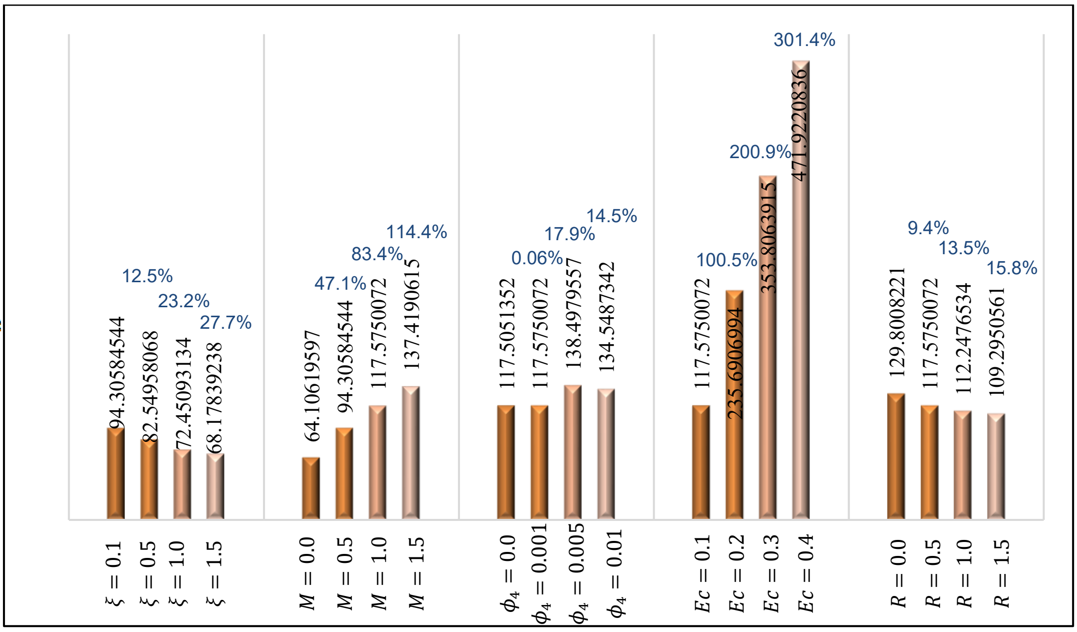

Figure 3. The Values of $Re_x^{-1/2}Nu_x$ for Several Parameters

It is eye-catching that varying ξ from 0.1 to 1.5 will diminuation the $Re_x^{-1/2}Nu_x$ about 27% which exposed in Fig. 3. The fluid displays stronger non-Newtonian behavior when ξ surges, predominantly boosted shear-thinning effects. This occurance give impact towards a decrease in the thermal conductivity near the surface and broader the thermal boundary layer, while further decline in the temperature gradient at the wall. Hence, the amplified flow resistance exacerbates thermal diffusion supremacy, added to plum the heat transfer efficiency.

The Lorentz force is generated with the applied M in the conducting fluid, where it used to be like a resistant body contradictory the fluid motion. $Re_x^{-1/2}Nu_x$ increases about 114% with an increase in the M from 0.0 to 1.5 as observed in Fig. 3. When stronger magnetic field is present, $Re_x^{-1/2}Nu_x$ is heighten at the sheet surface. This magnetic damping effect tends to suppress fluid motion and stabilize the boundary layer structure, especially near the surface. This suppression is coupled with boundary layer thinning, leading to a steeper temperature gradient at the wall where the suction is present. As a result, a more uniform and controlled thermal boundary layer is maintained, allowing the heat transfer rate to improve.

It is found that the $Re_x^{-1/2}Nu_x$ intensify by almost 14% with a growth in the ϕ_4 from 0.001 to 0.01 compared to ternary hybrid nanofluid ($\phi_4 = 0.0$), as exemplified in Fig. 3. This outcome highlights the important role of GO in improving the thermal performance of the nanofluid. By adding the ϕ_4 in the tetra hybrid mixture, the thermal conductivity of the nanofluid advances, leading to improve heat transfer from the sheet to the fluid. Subsequently, this resulting in a higher wall heat flux, which directly corresponds to a higher Nusselt number. This is by reason of the superior thermal conductivity and interfacial thermal transport characteristics of GO, which enable superior heat removal from the surface. Even at very low concentrations, GO suggestively progresses the nanofluid's thermal performance due to its high thermal conductivity, large surface area, and ability to form conductive pathways, which augment heat transfer without triggering large upsurges in viscosity or stability issues. Notably that the combination of Ag, CuO and Al_2O_3 enhance further the characteristics of tetra hybrid nanofluid. Ag always known as the highest thermal and electrical conductivity enabling rapid heat dispersion with smaller effect on viscosity while CuO contributes thermal energy storage and stability under heighten temperature and Al_2O_3 improving the dispersion and long-term stability suspension.

Fig, 3 demonstrating an increased Ec from 0.1 to 0.4, which characterizes the effect of viscous dissipation, leads to a substantial enhancement in the $Re_x^{-1/2}Nu_x$, with an estimated intensification of 300%. This infers that the kinetic energy of the flow is progressively converted into thermal energy due to internal friction, thereby uplifting the wall heat flux. The incidence of highly thermally conductive nanoparticles such as GO and Ag further amplifies this effect by facilitating efficient heat conduction away from the heated region, resulting in a sharper temperature gradient at the wall and consequently a higher heat transfer rate. These results highlight the vital role of viscous heating in improving heat transfer achievement in nanofluid-based thermal systems, predominantly under high-speed or high-friction flow conditions.

An augmented the radiation parameter (R) from 0.0 to 1.5 leads to a obvious drop in the $Re_x^{-1/2}Nu_x$, with a reduction of almost 15% is shown in Fig, 3. This result can be ascribed to the dominance of thermal radiation effects, which tend to redistribute the heat within the boundary layer and lower the temperature gradient near the wall. As R becomes more substantial, a portion of the thermal energy is radiated away rather than conducted through the fluid, thereby weakening the conductive heat transfer mechanism. Therefore, the wall heat flux diminutions, which is imitated in the lower $Re_x^{-1/2}Nu_x$.

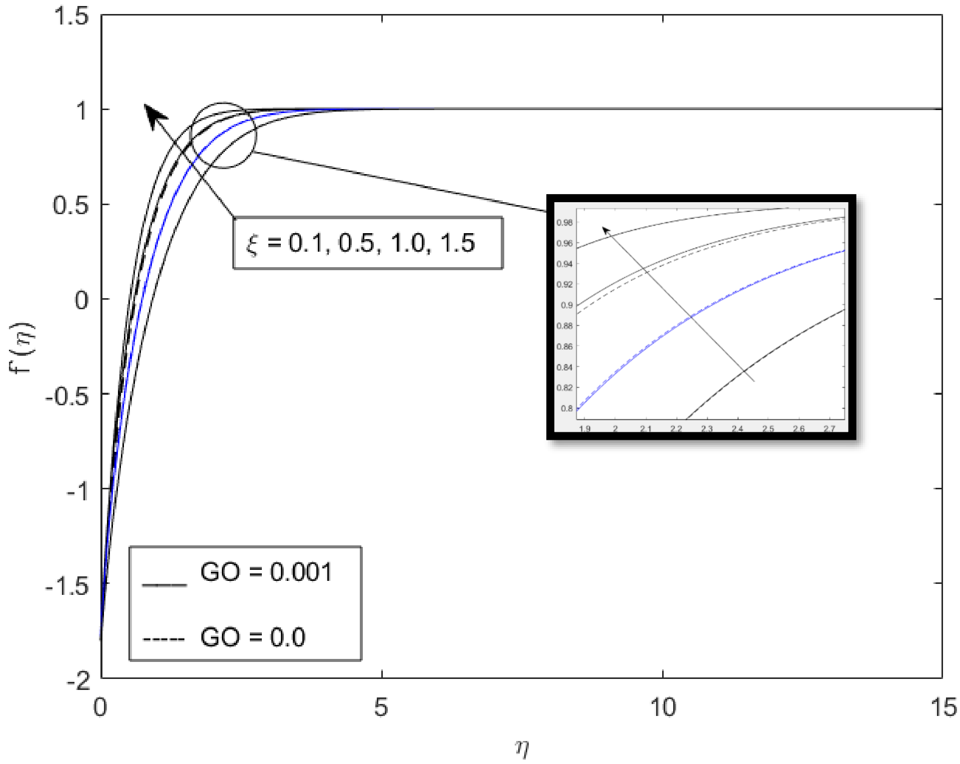

Figure 4. Disparity of Velocity with $\xi = 0.1, 0.5, 1.0, 1.5$

Based on Fig. 4, it is perceived that an improve in the ξ from 0.1 to 1.5 significantly upgrades the velocity profile. ξ characterizes shear-thinning behavior without singularity at zero shear rate, effectively shrinks the apparent viscosity of the fluid as this parameter rises. This decline in resistance facilitates smoother fluid motion, thereby arising the velocity within the boundary layer. Furthermore, the integration of GO nanoparticles into the tetra hybrid nanofluid substantially augments this effect. Nonetheless, the leading stimulate of ξ and the inclusion of GO clearly explains an upward trend in velocity, proving the favourable role of non-Newtonian characteristics and GO-based tetra hybrid nanofluids in developing flow behavior.

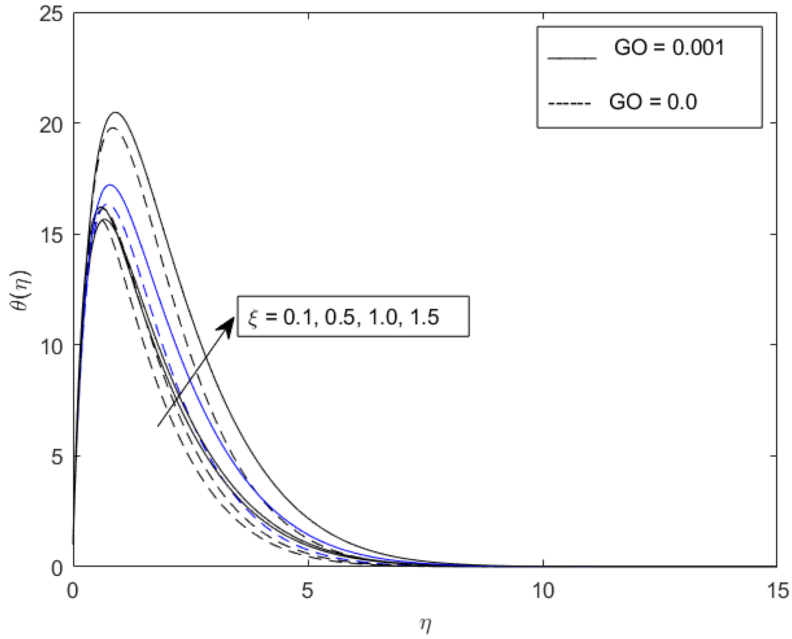

Figure 5. Disparity of Temperature with $\xi = 0.1, 0.5, 1.0, 1.5$

A higher ξ reduces the effective viscosity, which weakens the internal resistance and enhances thermal energy diffusion within the boundary layer. It is found that the temperature profile raises with the enhancement of the Powell–Eyring parameter as depicted in Fig. 5. This leads to a raise in the fluid temperature near the surface. GO has excellent thermal conductivity and a high surface-to-volume ratio, enabling it to store and transfer more thermal energy. Furthermore, the inclusion of GO in the tetra hybrid nanofluid substantially amplifies this thermal effect. As a result, nanofluids with GO exhibit higher temperature profiles compared to those without GO.

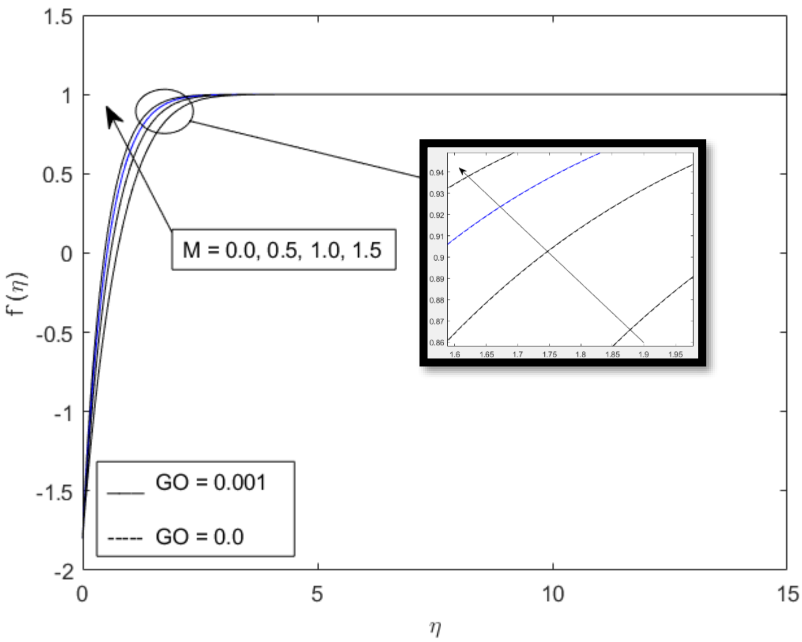

Figure 6. Disparity of Velocity with $M = 0.0, 0.5, 1.0, 1.5$

In Fig. 6, the intensification of velocity profile revealed when improvement in M from 0.0 to 1.5. The higher temperature arises because the magnetic field interacts with the electrically conducting nanofluid, which generates a Lorentz force. Furthermore, including graphene oxide (GO) in the tetra-hybrid nanofluid boosts the temperature slightly. This small increase is due to GO's high thermal conductivity and its superior ability to distribute thermal energy throughout the fluid. Ultimately, the results confirmed that M had the greatest impact on velocity, while GO independently caused a minor temperature increase, separate from any effects related to the magneto-hydrodynamics (MHD) and the advanced hybrid-nanofluid properties.

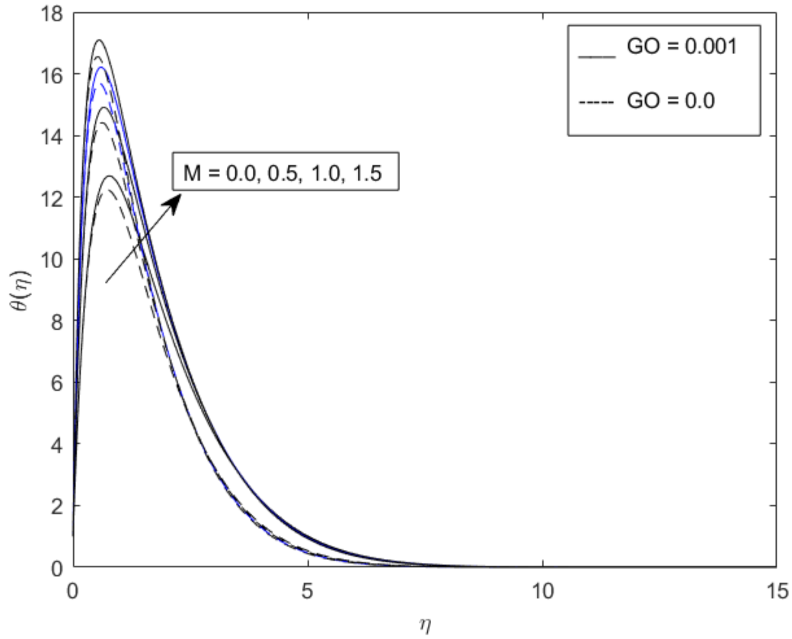

Figure 7. Disparity of Temperature with $M = 0.0, 0.5, 1.0, 1.5$

Fig. 7 clearly illustrates that as M increases, so does the temperature profile. This happens because M contacting the electrically conducting nanofluid enhances the Lorentz force. The resulting Lorentz force then generates Joule heating, which pumps more thermal energy into the boundary layer and ultimately raises the temperature. Furthermore, adding graphene oxide (GO) to the tetra-hybrid nanofluid results in higher temperatures compared to the non-GO version. This is due to the synergistic effect between GO and the metallic nanoparticles (like Ag, CuO, and Al_2O_3) in the ethylene glycol base fluid, which collectively improves the nanofluid's effective thermal conductivity. Overall, the data indicate that a stronger M and the inclusion of GO work together to boost the temperature distribution within the nanofluid flow.

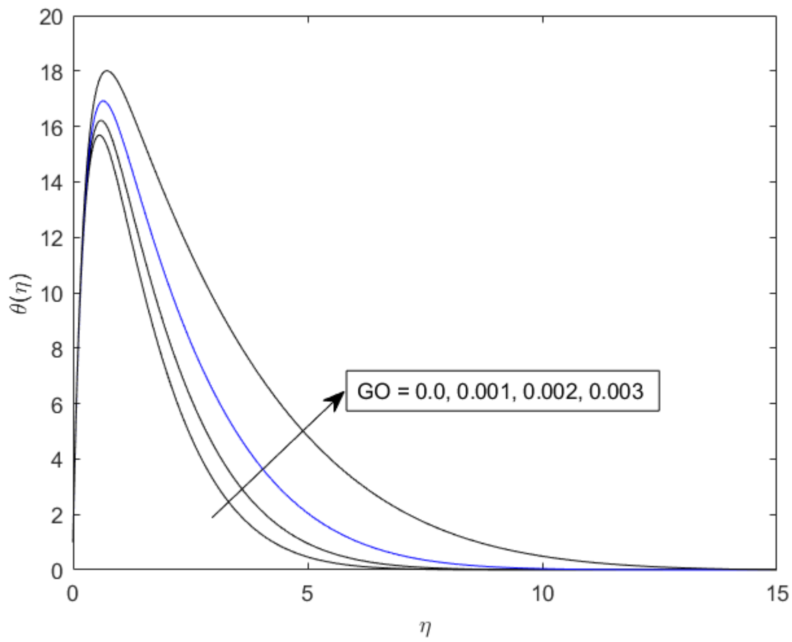

Figure 8. Disparity of Temperature with $\phi_4 = 0.0, 0.001, 0.002, 0.003$

From Fig. 8, the observation of a raise for ϕ_4 from 0.0 to 0.003 surpasses an intensification within the temperature profile along the boundary layer. This behavior can be accredited to the exceptional thermal conductivity of GO, which enhances the overall heat transport capability of the hybrid nanofluid. When ϕ_4 increases, the effective thermal conductivity of the tetra hybrid nanofluid improves, allowing more competent absorption and distribution of thermal energy. As a result, the thermal boundary layer becomes thicker, and the temperature near the surface increases. Additionally, the non-Newtonian behavior of the base fluid, modeled using the Powell–Eyring framework, along with the effect of Eckert number (representing viscous dissipation), thermal radiation, suction, and the shrinking sheet, further modifies the temperature field. The Eckert number contributes to internal heat generation through frictional heating, while radiation effects and shrinking dynamics influence the thermal gradient. Suction tends to reduce the thermal boundary layer, but its impact is offset by the enhanced thermal capacity due to the higher GO content.

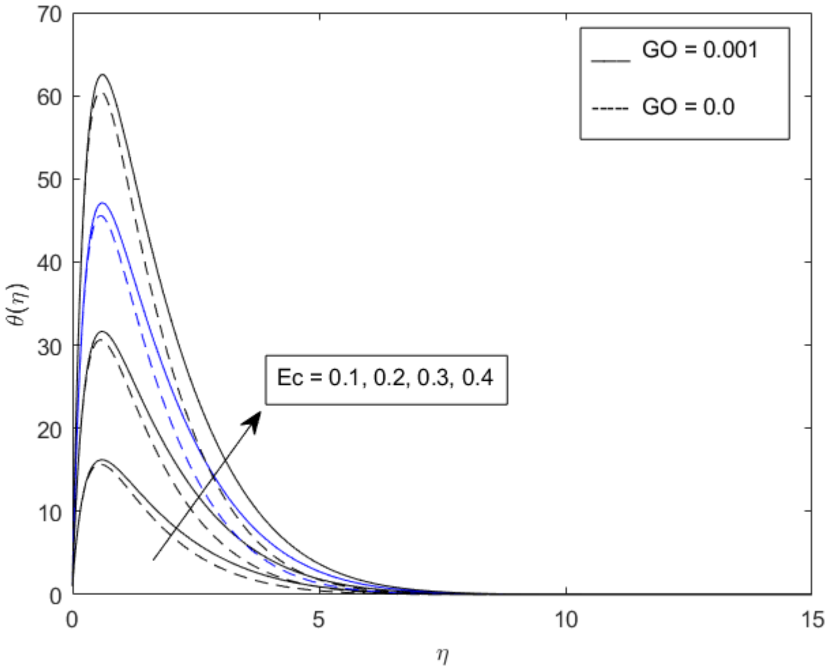

Figure 9. Disparity of Temperature with $Ec = 0.1, 0.2, 0.3, 0.4$

The analysis showed the amplification for the Ec from 0.1 to 0.4 surpasses in a significant intensify within the temperature profile, as illustrated in Fig. 9. Ec quantifies the ratio of kinetic energy to enthalpy and is closely associated with the consequence of viscous dissipation in the flow. As Ec increases, more kinetic energy is converted into internal energy due to frictional heating within the fluid layers, ensuing in a rise in fluid temperature. This phenomenon becomes more pronounced in non-Newtonian fluids such as those modeled by the Powell–Eyring framework, where shear-thinning effects can enhance internal resistance and heat generation. Furthermore, the presence of GO in the hybrid nanofluid amplifies the thermal response. GO possesses outstanding thermal conductivity, and its addition improves the nanofluid's capacity to retain and conduct heat, thus leading to higher temperatures compared to flows without GO.

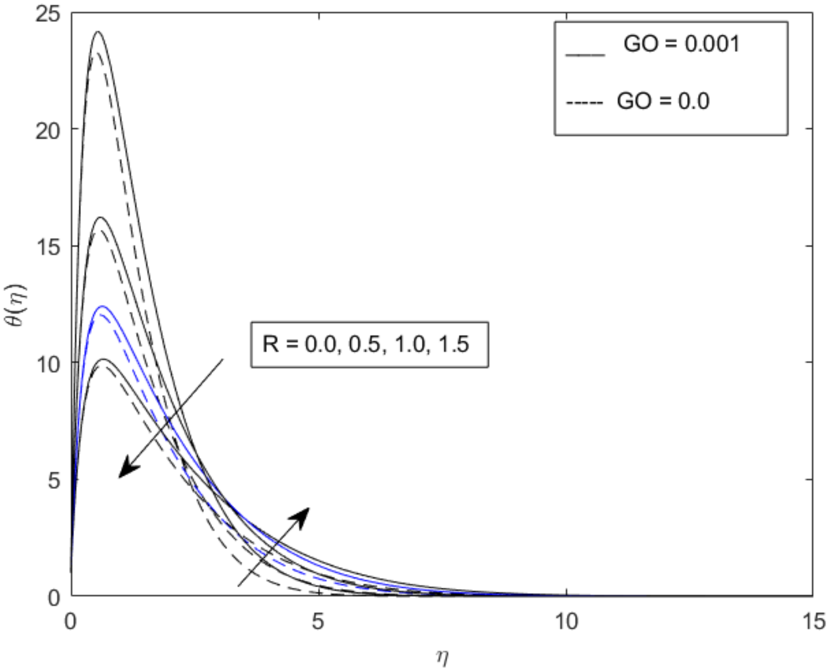

Figure 10. Disparity of Temperature with $R = 0.0, 0.5, 1.0, 1.5$

The effect of R on the temperature profile given in Fig. 10 reveals a non-monotonic behavior: an initial decrease in temperature is observed up to approximately $\eta = 3$, followed by a rise in temperature beyond this point. This behavior can be attributed to the dual role of radiative heat transfer. At lower values of the similarity variable η, R enhances energy loss from the surface, thus reducing the local temperature. However, as η increases, the accumulated thermal energy due to R begins to diffuse more uniformly throughout the boundary layer, leading to an overall rise in temperature in the far-field region. This trend is more pronounced in the presence of GO within the tetra hybrid nanofluid. GO's superior thermal conductivity improves heat distribution and energy retention in the fluid, thereby producing a consistently higher temperature profile compared to the non-GO counterpart.

4. CONCLUSION

Based on the numerical investigation presented in the numerical results, several significant conclusions can be drawn. The Powell–Eyring parameter notably increases skin friction and velocity, highlighting the enhanced shear stress and flow rate due to non-Newtonian fluid behavior. Similarly, an intensification in the magnetic parameter leads to higher skin friction and a modified velocity gradient; this is attributed to the Lorentz force which, in the context of a shrinking surface, provides a resistive force that assists the boundary layer in adhering to the sheet, thereby countering the shrinking motion. The inclusion and increasing concentration of GO within the tetra hybrid nanofluid moderately raises skin friction while significantly improving both thermal conductivity and flow velocity. In terms of heat transfer, the Powell–Eyring parameter reduces the Nusselt number, indicating a reduction in the rate of heat transfer, while the magnetic parameter enhances it. Notably, the Nusselt number increases by approximately 14% with higher GO concentration, affirming GO's superior thermal performance. The Eckert number plays a dominant role in thermal enhancement, with a dramatic 300% increase in the Nusselt number. This surge is physically justified by the intensified viscous dissipation and Joule heating, which rapidly convert mechanical and electrical energy into internal thermal energy, creating a steep temperature gradient at the wall. In contrast, a 15% reduction in the Nusselt number is observed as the radiation parameter increases, indicating radiative cooling effects. Temperature profiles show a consistent rise with increased Powell–Eyring, magnetic, Eckert, and GO concentration parameters. To evaluate the specific contribution of GO, a comparative analysis was performed between the tetra-hybrid mixture and a tri-hybrid (Ag–CuO–Al_2O_3/EG) baseline. The results indicate that the inclusion of GO (at ϕ_4= 0.001) independently raises the Nusselt number by approximately 14% compared to the tri-hybrid case. Interestingly, radiation causes the temperature to initially decrease up to η=3, followed by a rise beyond that point, illustrating the complex interplay of radiation with thermal boundary layer behavior. Among the four nanoparticles employed, graphene oxide (GO) is identified as the most effective contributor to the thermal enhancement. This is observed under high-heat flux conditions where GO's superior intrinsic thermal conductivity and large 2D surface-to-volume ratio create more efficient heat conduction pathways than the spherical metallic and ceramic counterparts. GO's high intrinsic thermal conductivity combined with its large specific surface area and excellent dispersion stability in ethylene glycol allows it to create efficient conductive pathways and maintain uniform suspension throughout the flow domain. The combination of GO's superior heat conduction and its synergistic interaction with metallic and oxide nanoparticles under magnetohydrodynamic and shrinking sheet conditions makes it the dominant factor in achieving enhanced heat transfer performance in this study. This study confirms that a minimal addition of GO nanoparticles to an Ag–CuO–Al_2O_3/EG base mixture provides substantial heat transfer enhancement, offering a cost-effective and stable tetra-hybrid nanofluid formulation for industrial cooling. The results are directly applicable to MHD-assisted heat exchangers, high-performance electronic cooling systems, and thermally managed renewable energy devices.

Author Contributions

Nooraini Zainuddin: Data Curation, Formal Analysis, Methodology. Nur Syahirah Wahid: Data Curation, Resources, Funding. Iskandar Waini: Methodology, Resources. Nor Ain Azeany Mohd Nasir: Software, Investigation, Validation, Writing-Review and Editing. Norihan Md Arifin: Supervision, Conceptualization. Norli Abdullah: Data Curation, Investigation. All authors discussed the results, contributed to the manuscript's preparation, and approved the final version of publication.

Funding Statement

This study was made possible through funding provided by Universiti Putra Malaysia under grant number GP-IPM 9787700.

Acknowledgment

The authors would like to extend their earnest gratitude to the Ministry of Higher Education Malaysia, Universiti Putra Malaysia, the National Defence University of Malaysia and Universiti Teknikal Malaysia Melaka for their generous support and contributions to this research endeavour.

Declarations

The authors declare that has no conflicts of interest to report study.

Declaration of Generative AI and AI-assisted technologies

The authors declare that no generative AI or AI-assisted technologies were used in the preparation of this manuscript, including for writing, editing, data analysis, or the creation of tables and figures.

REFERENCES

[1] I. Mahariq, D. Khan, H. Ali Ghazwani and M. Ali Shah, "ENHANCING HEAT AND MASS TRANSFER IN MHD TETRA HYBRID NANOFLUID ON SOLAR COLLECTOR PLATE THROUGH FRACTAL OPERATOR ANALYSIS," *Results in Engineering,* vol. 24, p. 103163, 2024. doi: https://doi.org/10.1016/j.rineng.2024.103163.

[2] S. Zainab, S. Shakir, N. Sher Akbar, K. Batool and T. Muhammad, "HEAT TRANSFER OPTIMIZATION USING COMPUTATIONAL INSIGHTS INTO NODAL/SADDLE POINT FLOW PATTERNS OF TERA-HYBRID NANOFLUID CONTAINING MICROBES IN A CYLINDRICAL SHELLS," *Case Studies in Thermal Engineering,* vol. 64, p. 105340, 2024. doi: https://doi.org/10.1016/j.csite.2024.105430.

[3] M. Mohamed Okash, M. Abbas, H. F. M. Ameen, F. Salah, A. Abbas, I. Khan, M. Ould Sidi, W. Rajhi and A. M. Galal, "APPLICATIONS OF CASSON TETRA HYBRID NANOFLUID IN INDUSTRIAL COOLING SYSTEMS: AN INVESTIGATION OF RADIATIVE FLOW AND STEPHAN BLOWING IMPACTS," *Journal of Radiation Research and Applied Sciences,* vol. 18, p. 101300, 2025. doi: https://doi.org/10.1016/j.jrras.2025.101300.

[4] K. Rafique, . Z. Mahmood, H. Abd El-Wahed Khalifa, E. A.A. Ismail, F. A. Awwad, A. Kumar and S. Sh Tantawy, "THERMAL AND FLOW CHARACTERISTICS OF TETRA-HYBRID NANOFLUID OVER A STRETCHING/SHRINKING INCLINED CYLINDER: INFLUENCE OF HEAT ABSORPTION AND QUADRATIC RADIATION," *Journal of Radiation Research and Applied Sciences,* vol. 18, p. 101513, 2025. doi: https://doi.org/10.1016/j.jrras.2025.101513.

[5] N. S. Khashi'ie, M. F. Mukhtar, M. F. Bin Abdollah, N. Md Arifin and I. Pop, "RESPONSE SURFACE-BASED OPTIMIZATION AND SENSITIVITY ANALYSIS OF MHD TETRA HYBRID NANOFLUID FLOW OVER A SHRINKING DISK," *Chinese Journal of Physics,* vol. 96, pp. 228-244, 2025. doi: https://doi.org/10.1016/j.cjph.2025.05.013.

[6] Z. Arshad, . E. Ghandourah, M. A. Zahoor Raja, Z. Shah, . A. Ali Pasha, S. Khadam Hussain, W. Azeem Khan and M. M. Alam, "ARTIFICIAL INTELLIGENCE-BASED PROCEDURE TO ANALYZE HEAT TRANSFER FEATURES FOR CHEMICALLY REACTIVE DARCY-FORCHHEIMER FLOW OF MAGNETIZED TETRA-HYBRID NANOFLUID FLOW CAPTURING JOULE HEATING ASPECTS THROUGH STENOTIC ARTERY," *Tribology International,* vol. 206, p. 110532, 2025. doi: https://doi.org/10.1016/j.triboint.2025.110532.

[7] M. Abbas, S. Shomurotova, Q. Al-Mdallal, A. Akgül, Z. Jastaneya and H. AL Garalleh, "COMPARATIVE ANALYSIS OF HALL CURRENT IMPACT ON MHD LAMINAR SURFACE TENSION GRADIENT 3D FLOW OF PROPYLENE GLYCOL BASED TETRA HYBRID NANOFLUID WITH GENERALIZED FICK'S AND FOURIER'S PERSPECTIVE," *International Journal of Thermofluids,* vol. 26, p. 101003, 2025 doi:. https://doi.org/10.1016/j.ijft.2025.101083.

[8] A. M. Galal, I. Khan, M. Abbas, A. A. Faqihi and M. Saqlain Sajjad, "THERMAL RADIATION AND LOCAL THERMAL NON-EQUILIBRIUM EFFECTS ON MHD CHEMICAL REACTIVE FLOW OF TETRA HYBRID NANOFLUID WITH VELOCITY SLIP CONDITIONS," *Journal of Radiation Research and Applied Sciences,* vol. 18, p. 101405, 2025 doi:. https://doi.org/10.1016/j.jrras.2025.101405.

[9] T. Sajid, . W. Jamshed, M. R. Eid, G. Cieza Altamirano, F. Aslam, A. Mahal Alanzi and A. Abd-Elmonem, "MAGNETIZED CROSS TETRA HYBRID NANOFLUID PASSED A STENOSED ARTERY WITH NONUNIFORM HEAT SOURCE (SINK) AND THERMAL RADIATION: NOVEL TETRA HYBRID TIWARI AND DAS NANOFLUID MODEL," *Journal of Magnetism and Magnetic Materials,* vol. 569, p. 170443, 2023. doi: https://doi.org/10.1016/j.jmmm.2023.170443.

[10] T. Sajid, . W. Jamshed, S. Algarni, T. Alqahtani, M. R. Eid, K. Irshad, G. C. Altamirano, S. M. El Din and K. W. Nahar Tajer, "CATALYSIS REACTION INFLUENCE ON 3D TETRA HYBRID NANOFLUID FLOW VIA OIL RIG SOLAR PANEL SHEET: CASE STUDY TOWARDS OIL EXTRACTION," *Case Studies in Thermal Engineering,* vol. 49, p. 103261, 2023. doi: https://doi.org/10.1016/j.csite.2023.103261.

[11] M. Abbas, R. Marzouki, H. F. M. Ameen, A. Dilsora, J. Younis and A. Akgül, "PERFORMANCE OF MAGNETIC DIPOLE CONTRIBUTION ON ELECTROMAGNETIC ELLIS TETRA HYBRID NANOFLUID WITH THE APPLICATIONS OF SURFACE TENSION GRADIENT: A XUE MODEL EXPLORATION," *International Journal of Thermofluids,* vol. 24, p. 100951, 2024. doi: https://doi.org/10.1016/j.ijft.2024.100951.

[12] P. Paul and S. D. Das, "ELECTRO-PUMPING PARADIGM OF NON-NEWTONIAN BLOOD WITH TETRA-HYBRID NANOPARTICLES INFUSION IN A CILIATED ARTERY," *Chinese Journal of Physics,* vol. 87, pp. 195-231, 2024. doi: https://doi.org/10.1016/j.cjph.2023.12.008.

[13] T. Kanti Das, A. Paul, J. Mani Nath and N. Sarma, "THE YAMADA-OTA MODEL-BASED CASSON QUADRA HYBRID NANOFLUID STAGNATION FLOW CONFIGURED BY OHMIC HEATING, HEAT SOURCE, AND NEWTONIAN BOUNDARY HEATING ACROSS AN EXPONENTIALLY STRETCHED CYLINDER," *Partial Differential Equations in Applied Mathematics,* vol. 14, p. 101159, 2025. doi: https://doi.org/10.1016/j.padiff.2025.101159.

[14] M. Amudhini and P. De, "IRREVERSIBILITY ANALYSIS ON TETRA-HYBRID NON-NEWTONIAN FLUIDS WITH THERMAL RADIATION AND SORET-DUFOUR EFFECTS OVER POROUS INCLINED STRETCHING SHEET," *Results in Engineering,* vol. 26, p. 104786, 2025. doi: https://doi.org/10.1016/j.rineng.2025.104786.

[15] N. Fatima, M. Kallel, N. Ijaz, A. Zeeshan and N. Saleem, "THERMODYNAMIC ANALYSIS AND ENTROPY GENERATION OF ELECTROOSMOTIC TETRA-HYBRID NANOPARTICLE TRANSPORT IN COMPLEX BIOLOGICAL TRANSPORT," *Results in Engineering,* vol. 25, p. 104308, 2025. doi: https://doi.org/10.1016/j.rineng.2025.104308.

[16] D. Khan, P. Kumam, P. Suttiarporn and T. Srisurat, "FOURIER'S AND FICK'S LAWS ANALYSIS OF COUPLE STRESS MHD SODIUM ALGINATE BASED CASSON TETRA HYBRID NANOFLUID ALONG WITH POROUS MEDIUM AND TWO PARALLEL PLATES," *South African Journal of Chemical Engineering,* vol. 47, pp. 279-290, 2024. doi: https://doi.org/10.1016/j.sajce.2023.12.003.

[17] N. Elboughdiri, U. Nazir, M. Sohail and A. A. A. Mousa, "COMBINE THERMAL PERFORMANCE BASED ON DUST PARTICLES AND HALL AND ION SLIP CURRENTS INCLUDING TETRA-HYBRID NANOPARTICLES ON HOWARTH'S WAVY PIPE," *Results in Engineering,* vol. 23, p. 102666, 2024. doi: https://doi.org/10.1016/j.rineng.2024.102666.

[18] A. Hussain Majeed, A. Zubair Jan, A. M. Alamri, S. A. AlQahtani, M. R. Ali and A. S. Hendy, "RECENT DEVELOPMENTS IN THE DARCY-FORCHHEIMER MODEL OF MAGNETIZED TETRA HYBRID NANOFLUID ACTIVATION ENERGY/JOULE HEATING IN A STENOTIC ARTERY," *Case Studies in Thermal Engineering,* vol. 59, p. 104346, 2024. doi: https://doi.org/10.1016/j.csite.2024.104346.

[19] N. Gomathi and D. Poulomi, "ENTROPY OPTIMIZATION ON EMHD CASSON WILLIAMSON PENTA-HYBRID NANOFLUID OVER POROUS EXPONENTIALLY VERTICAL CONE," *Alexandria Engineering Journal,* vol. 2024, pp. 590-610, 2024. doi: https://doi.org/10.1016/j.aej.2024.07.092.

[20] S. Yuan, Y. Leng, A. Fouly, E. Mahrous Awwad, U. Nazir and M. Sohail, "A STUDY OF FOUR-PHASE FLUID AND THERMAL ENHANCEMENT BASED ON TETRA-HYBRID NANOFLUID CONSIDERING TEMPERATURE JUMP ON A SPINNING SPHERE," *Case Studies in Thermal Engineering,* vol. 58, p. 104353, 2024. doi: https://doi.org/10.1016/j.csite.2024.104353.

[21] M. Dinesh kumar , J. L. Díaz Palencia, G. Dharmaiah, A. Wakif , S. Noeiaghdam, U. Fernandez-Gamiz and S. Dinarvand, "ANFIS-PSO ANALYSIS ON AXISYMMETRIC TETRA HYBRID NANOFLUID FLOW OF CU-CNT-GRAPHENE-TIO2 WITH WEG-BLOOD UNDER LINEAR THERMAL RADIATION AND INCLINED MAGNETIC FIELD: A BIO-MEDICINE APPLICATION," *Heliyon,* vol. 11, no. 1, p. e41429, 2025. doi: https://doi.org/10.1016/j.heliyon.2024.e41429.

[22] H. T. Basha, R. Sivaraj and B. Jang, "ENTROPY ANALYSIS AND HYDROTHERMAL BEHAVIOR OF MAGNETOHYDRODYNAMIC MOS2–FE3O4/H2O HYBRID NANOFLUID FLOW DRIVEN BY BUOYANCY IN A SQUARE ENCLOSURE WITH DIVERSE FIN HEIGHTS," *Physics of Fluids,* vol. 35, no. 12, p. 122003, 2023. doi: https://doi.org/10.1063/5.0177860.

[23] K. Thirumalaisamy and A. Subramanyam Reddy, "NUMERICAL COMPUTATION ON MHD NATURAL CONVECTIVE TERNARY NANOFLUID FLOW AND HEAT TRANSFER IN A POROUS SQUARE CAVITY: MARKER-AND-CELL TECHNIQUE," *International Journal of Numerical Methods for Heat & Fluid Flow,* vol. 33, no. 10, p. 3425–3466, 2023. doi: https://doi.org/10.1108/HFF-04-2023-0167.

[24] K. Thirumalaisamy , Y. D. Lee and H. Kim, "MAGNETOHYDRODYNAMIC BUOYANCY-DRIVEN HYBRID NANOFLUID FLOW AND HEAT TRANSFER WITHIN A PARTIALLY HEATED POROUS SQUARE CAVITY," *Physic of Fluids,* vol. 37, p. 042011, 2025. doi: https://doi.org/10.1063/5.0264031.

[25] H. Kim, Y. Do, S. Ramachandran, M. Sankar and K. Thirumalaisamy, "COMPUTATIONAL ANALYSIS OF MAGNETOHYDRODYNAMIC TERNARY-HYBRID NANOFLUID FLOW AND HEAT TRANSFER INSIDE A POROUS CAVITY WITH SHAPE EFFECTS," *Physics of Fluids,* vol. 36, p. 082008, 2024. doi: https://doi.org/10.1063/5.0222802.

[26] P. Paul, P. Karmakar , S. Das and S. Das, "DEMONSTRATION OF ANGIOPLASTY USING A BALLOON CATHETER IN TETRA-HYBRID NANO-BLOODSTREAM WITHIN AN ELECTRIFIED STENOTIC ARTERIAL CAVITY UNDER A MAGNETIC FIELD: ARTIFICIAL NEURAL NETWORK ANALYSIS," *Biomedical Signal Processing and Control,* vol. 96, no. B, p. 106549, 2024. doi: https://doi.org/10.1016/j.bspc.2024.106549.

[27] F. Mumtaz, A. Al-Zubaidi, T. Abbas and S. Saleem, "THERMAL PERFORMANCE ANALYSIS OF QUATERNARY HYBRID NANOFLUIDS WITH RADIATIVE AND JOULE HEATING EFFECTS IN MAGNETOHYDRODYNAMIC FLOW OVER A STRETCHED SURFACE," *Results in Physics,* vol. 71, p. 108176, 2025. doi: https://doi.org/10.1016/j.rinp.2025.108176.

[28] S. Swami, S. Biradar, J. V. Tawade, N. V. Kulkarni, B. S. Abdullaeva, D. Mohammad Khidhir, N. Batool and T. Saidani, "HEAT AND MASS TRANSFER ANALYSIS OF WILLIAMSON NANOFLUIDS UNDER THE INFLUENCE OF MAGNETIC FIELD AND JOULE'S HEATING," *Partial Differential Equations in Applied Mathematics,* vol. 13, p. 101148, 2025. doi: https://doi.org/10.1016/j.padiff.2025.101148.

[29] G. Kanaka Lakshmi and P. S. Ramachandra Murty, "IMPACT OF HALL CURRENT AND ROTATIONAL ON MHD FLOW OF NANOFLUID WITH JOULE HEATING AND VISCOUS DISSIPATION," *International Journal of Thermofluids,* vol. 27, p. 101153, 2025. doi: https://doi.org/10.1016/j.ijft.2025.101153.

[30] Y. Wang, L. Yu, . A. Obalalu, U. Khan, M. Waqas, A. Elrashidi and M. Zakarya, "DISSIPATIVE HEAT TRANSFER IN BLOOD-BASED TERNARY HYBRID NANOFLUIDS THROUGH A PARALLEL CHANNEL WITH ENTROPY OPTIMIZATION: THE CASE OF BIOMEDICAL APPLICATIONS," *Alexandria Engineering Journal,* vol. 115, pp. 252-263, 2025. doi: https://doi.org/10.1016/j.aej.2024.12.026.

[31] A. Tanveer, I. M. Z. Alqarni, S. Saleem and A. Al-Zubaidi, "ENHANCEMENT IN HEAT GENERATION THROUGH TERNARY HYBRID NANOFLUID IN A PERIODIC CHANNEL," *Case Studies in Thermal Engineering,* vol. 69, p. 106011, 2025. doi: https://doi.org/10.1016/j.csite.2025.106011..

[32] J. Iqbal, F. M. Abbasi and M. M. Alam, "THERMAL ENHANCEMENT AND ENERGY MINIMIZATION WITH DIHYDROGEN OXIDE-BASED NANOFLUIDS," *International Journal of Hydrogen Energy,* vol. 113, pp. 585-598, 2025. doi: https://doi.org/10.1016/j.ijhydene.2025.02.454.

[33] D. Safa, S. Mohamed Rafik , F. Lafta Rashid, D. Hacen, M. Abdallah, K. Mohamed, I. Khan, M. Sabaoon Khan and B. Almaz Ali Yousif, "THERMALLY RADIATIVE MHD JEFFERY-HAMEL FLOW IN A CONVERGENT-DIVERGENT CONDUIT: A HYBRID NANOFLUID FLUID MODEL UNDER NANOPARTICLES SHAPE FACTOR IMPACT," *Journal of Radiation Research and Applied Sciences,* vol. 18, no. 1, p. 101314, 2025. doi: https://doi.org/10.1016/j.jrras.2025.101314

[34] [Online]. Available: https://www.mathworks.com/help/matlab/ref/bvp4c.html.

[35] N. A. Aminuddin, N. A. A. Mohd Nasir, N. Abdullah and W. Jamshed, "ANALYSIS OF GO-MOS2/EG POWELL-EYRING FLUID TRANSPORATION IN STAGNATION POINT FLOW AND HEAT TRANSFER OVER A SHRINKING SURFACE," *Journal of Advance Research in Fluid Mechanics and Thermal Sciences,* vol. 112, no. 2, pp. 1-13, 2023. doi: https://doi.org/10.37934/arfmts.112.2.113.

[36] I. Waini, A. Ishak and I. Pop, "EYRING-POWELL FLUID FLOW PAST A SHRINKING SHEET: EFFECT OF MAGNETOHYDRODYNAMIC (MHD) AND JOULE HEATING," *Journal of Advance Research in Fluid Mechanics and Thermal Sciences,* vol. 116, no. 1, pp. 64-77, 2024. doi: https://doi.org/10.37934/arfmts.116.1.6477.

[37] K. Azeez, A. F. Hameed and A. M. Hussein, "NANOFLUID HEAT TRANSFER AUGMENTATION IN A DOUBLE PIPE HEAT EXCHANGER," *AIP Conference Proceedings,* vol. 2213, p. 020059, 2020. doi: https://doi.org/10.1063/5.0000243.

[38] S. Abu Bakar, N. Md Arifin, N. Bachok and F. Md Ali, "EFFECT OF THERMAL RADIATION AND MHD ON HYBRID AG-TIO2/H2O NANOFLUID PAST A PERMEABLE POROUS MEDIUM WITH HEAT GENERATION," *Case Studies in Thermal Engineering,* vol. 28, p. 101681, 2021. doi: https://doi.org/10.1016/j.csite.2021.101681.

[39] J. Fal, M. Wanic, G. Budzik, M. Oleksy and G. Żyła, "ELECTRICAL CONDUCTIVITY AND DIELECTRIC PROPERTIES OF ETHYLENE GLYCOL-BASED NANOFLUIDS CONTAINING SILICON OXIDE-LIGNIN HYBRID PARTICLES," *Nanomaterials,* vol. 9, no. 7, p. 1008, 2019. doi: https://doi.org/10.3390/nano9071008.

[40] M. Liu, . M. C. Lin and C. Wang, "ENHANCEMENTS OF THERMAL CONDUCTIVITIES WITH CU, CUO, AND CARBON NANOTUBE NANOFLUIDS AND APPLICATION OF MWNT/WATER NANOFLUID ON A WATER CHILLER SYSTEM," *Nanoscale Research Letters,* vol. 6, p. 297, 2011. doi: https://doi.org/10.1186/1556-276X-6-297.

[41] B. Takabi and S. Salehi, "AUGMENTATION OF THE HEAT TRANSFER PERFORMANCE OF A SINUSOIDAL CORRUGATED ENCLOSURE BY EMPLOYING HYBRID NANOFLUID," *Advances in Mechanical Engineering,* vol. 2014, p. 147059, 2014. doi: https://doi.org/10.1155/2014/147059.

[42] R. Cortell, "HEAT AND FLUID FLOW DUE TO NON-LINEARLY STRETCHING SURFACES," *Applied Mathematics and Computation,* vol. 217, pp. 7564-7572, 2011. doi: https://doi.org/10.1016/j.amc.2011.02.029.

[43] A. Srivastava, A. Kumar and A. Chandra Pandey, "FLOW AND HEAT TRANSFER OF NON-MISCIBLE MICROPOLAR AND NEWTONIAN FLUID IN POROUS CHANNEL SANDWICHED BETWEEN PARALLEL PLATES," *Chinese Journal of Physics,* vol. 92, pp. 33-50, 2024. doi: https://doi.org/10.1016/j.cjph.2024.08.041.

[44] H. Ma, B. He, L. Su and D. He, "HEAT TRANSFER ENHANCEMENT OF NANOFLUID FLOW AT THE ENTRY REGION OF MICROTUBES," *International Journal of Thermal Sciences,* vol. 184, p. 107944, 2023. doi: https://doi.org/10.1016/j.ijthermalsci.2022.107944.

[45] T. Balaji, D. Mohan Lal and C. Selvam, "A CRITICAL REVIEW ON THE THERMAL TRANSPORT CHARACTERISTICS OF GRAPHENE-BASED NANOFLUIDS," *Energies,* vol. 16, no. 6, p. 2663, 2023. doi: https://doi.org/10.3390/en16062663.